J. Fluid Mech. (2000), *vol.* 407, *pp.* 291–314. Printed in the United Kingdom

Stability of fluid flow in a flexible tube to non-axisymmetric disturbances

By V. SHANKAR AND V. KUMARAN

Department of Chemical Engineering, Indian Institute of Science, Bangalore 560 012, India

(Received 17 June 1998 and in revised form 25 October 1999)

The stability of fluid flow in a flexible tube to non-axisymmetric perturbations is analysed in this paper. In the first part of the paper, the equivalents of classical theorems of hydrodynamic stability are derived for inviscid flow in a flexible tube subjected to arbitrary non-axisymmetric disturbances. Perturbations of the form $v_i = \tilde{v}_i \exp[ik(x - ct) + in\theta]$ are imposed on a steady axisymmetric mean flow $U(r)$ in a flexible tube, and the stability of mean flow velocity profiles and bounds for the phase velocity of the unstable modes are determined for arbitrary values of azimuthal wavenumber n. Here r, θ and x are respectively the radial, azimuthal and axial coordinates, and k and c are the axial wavenumber and phase velocity of disturbances. The flexible wall is represented by a standard constitutive relation which contains inertial, elastic and dissipative terms. The general results indicate that the fluid flow in a flexible tube is stable in the inviscid limit if the quantity $U\mathrm{d}\mathcal{G}/\mathrm{d}r \geqslant 0$, and could be unstable for $U\mathrm{d}\mathcal{G}/\mathrm{d}r < 0$, where $\mathcal{G} \equiv rU'/(n^2 + k^2r^2)$. For the case of Hagen–Poiseuille flow, the general result implies that the flow is stable to axisymmetric disturbances ($n = 0$), but could be unstable to non-axisymmetric disturbances with any non-zero azimuthal wavenumber ($n \neq 0$). This is in marked contrast to plane parallel flows where two-dimensional disturbances are always more unstable than three-dimensional ones (Squire theorem). Some new bounds are derived which place restrictions on the real and imaginary parts of the phase velocity for arbitrary non-axisymmetric disturbances.

In the second part of this paper, the stability of the Hagen–Poiseuille flow in a flexible tube to non-axisymmetric disturbances is analysed in the high Reynolds number regime. An asymptotic analysis reveals that the Hagen–Poiseuille flow in a flexible tube is unstable to non-axisymmetric disturbances even in the inviscid limit, and this agrees with the general results derived in this paper. The asymptotic results are extended numerically to the moderate Reynolds number regime. The numerical results reveal that the critical Reynolds number obtained for inviscid instability to non-axisymmetric disturbances is much lower than the critical Reynolds numbers obtained in the previous studies for viscous instability to axisymmetric disturbances when the dimensionless parameter $\Sigma = \rho GR^2/\eta^2$ is large. Here G is the shear modulus of the elastic medium, ρ is the density of the fluid, R is the radius of the tube and η is the viscosity of the fluid. The viscosity of the wall medium is found to have a stabilizing effect on this instability.

1. Introduction

The present study addresses the stability of fluid flow in a flexible tube to non-axisymmetric disturbances. An important difference between the stability of flow

through plane channels and axisymmetric tubes is that a result similar to the Squire theorem, which states that two-dimensional disturbances are always more unstable than three-dimensional disturbances in a plane channel, cannot be derived for the flow in a tube. Consequently, it is necessary to study both axisymmetric and non-axisymmetric disturbances to determine the stability limits for the flow in a tube. Previous studies on the stability of flow through a flexible tube were restricted to axisymmetric disturbances. The salient results of these studies are enumerated below.

(*a*) The Hagen–Poiseuille flow in a flexible tube could become unstable even in the limit of zero Reynolds number (Kumaran 1995*a*) when the dimensionless velocity ($V\eta/GR$) increases beyond a critical value. Here, V is the maximum velocity in the tube, η is the fluid viscosity, G is the modulus of elasticity of the wall material and R is the tube radius. This class of modes are referred to as 'viscous modes'.

(*b*) The Hagen–Poiseuille flow is always stable to high Reynolds number axisymmetric inviscid modes (Kumaran 1995*b*). These modes are referred to as 'regular inviscid modes'. This analysis is not conclusive, however, and non-axisymmetric disturbances in a flexible tube could become unstable in the high Reynolds number limit.

(*c*) There is the possibility of the Hagen–Poiseuille flow becoming unstable in the limit of high Re, and the instability mechanism is a continuation of the low Re axisymmetric viscous unstable modes (Kumaran 1998*a*) to high Reynolds number. The critical Reynolds number in this case scales as $Re \propto \Sigma^{\alpha}$, where the exponent α is between 0.7 and 0.75. Here, $\Sigma = (\rho G R^2/\eta^2)$, where ρ is the fluid density.

(*d*) There is another class of modes, called the wall modes (Kumaran 1998*b*), where the vorticity is confined to a boundary layer of thickness $O(Re^{-1/3})$ at the wall of the tube. These modes also become unstable in the high Reynolds number limit. The critical Reynolds number in this case also scales as $Re \propto \Sigma^{\alpha}$, where the exponent α is between 0.7 and 0.75.

(*e*) Velocity profiles very different from the parabolic Hagen–Poiseuille flow, such as the developing flow and the converging flow in a flexible tube, could become unstable to axisymmetric disturbances even in the limit of infinite Re (Shankar & Kumaran 1999), and this instability is qualitatively different from the axisymmetric viscous instability of the Hagen–Poiseuille flow. The critical Reynolds number in this case scales as $Re \propto \Sigma^{1/2}$. These modes are referred to as 'singular inviscid modes'.

In the limit of high Reynolds number, there are a number of general results due to Rayleigh, Fjørtoft, Howard and Høiland (Drazin & Reid 1981) which predict potentially unstable velocity profiles and provide bounds on the wave speed of the unstable mode for two-dimensional flows bounded by rigid walls. Howard & Gupta (1962) have extended the classical theorems to inviscid flow of a Newtonian fluid between coaxial rigid cylinders, where the base flow velocity has both axial and 'swirl' (azimuthal) components; Maslowe (1974) has derived similar theorems for Poiseuille flow in a rigid pipe. The stability of inviscid flow is very sensitive to the boundary conditions at the surface, and the stability of flow near a rigid surface is very different from that near a flexible surface. The classical theorems of hydrodynamic stability are not applicable for flow in a flexible channel because a non-zero normal velocity is permitted at the wall. Yeo & Dowling (1987) and Yeo (1994) analysed the stability of inviscid flows in channels with passive compliant walls. A general constitutive equation for a compliant wall was derived using a variational-Lagrangian formulation, and this was used to relate the fluid velocity and stress at the wall. They derived bounds on the real and imaginary parts of the phase velocity and they showed that the bounds were consistent with some experimental observations. The classical theorems of hydrodynamic stability were modified and extended to inviscid flow in a flexible

tube by Kumaran (1996) in two limiting cases: axisymmetric modes and 'highly non-axisymmetric modes' where gradients in the azimuthal direction are much larger than the gradients in the axial direction. The generalization of classical theorems indicated that the Hagen–Poiseuille velocity profile in a flexible tube could become unstable to 'highly non-axisymmetric' disturbances.

In § 2, the classical theorems are modified and extended to inviscid flow in a flexible tube to arbitrary non-axisymmetric disturbances, and this part of the paper augments the analysis of Kumaran (1996) by removing the restriction on the 'highly non-axisymmetric' nature of the disturbances. The general results of § 2 indicate that the Hagen–Poiseuille flow could become unstable in a flexible tube in the inviscid limit, and this provides the motivation for the second part of the present work (§ 3). In § 3, the stability of the Hagen–Poiseuille flow to non-axisymmetric disturbances is analysed in the limit of high Reynolds number. A previous study by the authors (Shankar & Kumaran 1999) had shown that the developing flow in a flexible tube could become unstable to axisymmetric disturbances in the inviscid limit, and this instability was found to persist at *Re* as low as 100. Importantly, the critical *Re* for non-parabolic velocity profiles could be much lower than that for a parabolic velocity profile. The mechanism of instability of the developing flow profile to axisymmetric disturbances is qualitatively different from that of Hagen–Poiseuille flow to axisymmetric disturbances in the limit of high Reynolds number due to the presence of a 'critical layer' in the case of a developing flow. A critical layer is also present in the stability of Hagen–Poiseuille flow subjected to non-axisymmetric disturbances, and this qualitatively alters the nature of instability in the limit of high Reynolds number. Consequently, it is of interest to determine the critical Reynolds number for the Hagen–Poiseuille profile to non-axisymmetric disturbances, and to examine whether this is lower than that for the viscous instability of axisymmetric disturbances analysed in Kumaran (1998*a*).

In this paper, an asymptotic analysis is carried out in the limit of high *Re* (§ 3.1), and this analysis shows that the parabolic flow is indeed unstable to non-axisymmetric disturbances in the inviscid limit. A numerical solution of the complete governing equations is used to extend the high-*Re* asymptotic solutions to the moderate Reynolds number regime (§ 3.2). The numerical results (§ 3.3) reveal that the critical Reynolds number for the continuation of inviscid instability to non-axisymmetric disturbances is much lower than the critical *Re* for viscous instability to axisymmetric disturbances (Kumaran 1998*a*) when the dimensionless parameter characterizing the flexible tube $\Sigma \equiv \rho G R^2/\eta^2$ is large. In marked contrast, the parabolic flow in a rigid tube is stable to both axisymmetric and non-axisymmetric disturbances (Garg & Rouleau 1972; Salwen & Grosch 1972). Thus, the instability of parabolic flow to non-axisymmetric disturbances in a flexible tube predicted in this paper is qualitatively different from the stability of fluid flow in a rigid tube.

2. Generalization of classical theorems

The system consists of an incompressible Newtonian fluid of density ρ flowing through a tube of radius R whose walls are made of a flexible material. The only restriction placed on the laminar velocity profile $U(r)$ is that it decreases to zero at the wall. The perturbation to the velocity field has components (v_r, v_θ, v_x) along the radial (r), axial (x) and azimuthal (θ) directions in a cylindrical coordinate system of the form $v_i = \tilde{v}_i(r) \exp[\mathrm{i}k(x - ct) + \mathrm{i}n\theta]$. Here, $n = 0$ corresponds to axisymmetric disturbances and $n > 0$ for non-axisymmetric disturbances. The linearized mass and

momentum equations for the inviscid flow are

$$(\mathrm{d}_r + r^{-1})\tilde{v}_r + r^{-1}\mathrm{i}n\tilde{v}_\theta + \mathrm{i}k\tilde{v}_x = 0, \quad \mathrm{i}k(U-c)\tilde{v}_r + \mathrm{d}_r\tilde{p} = 0, \tag{2.1}$$

$$\mathrm{i}k(U-c)\tilde{v}_\theta + \mathrm{i}nr^{-1}\tilde{p} = 0, \quad \mathrm{i}k(U-c)\tilde{v}_x + U'\tilde{v}_r + \mathrm{i}k\tilde{p} = 0. \tag{2.2}$$

Here and in what follows, $\mathrm{d}_r \equiv \mathrm{d}/\mathrm{d}r$ and a prime also indicates differentiation with respect to r. The fluid density ρ does not explicitly appear in the above equations because the pressure has been scaled by the density. In the following analysis, all quantities are scaled by an appropriate combination of the density ρ, a velocity scale of the mean flow U_{max} and the radius of the tube R, so that all equations are dimensionless. The axial and azimuthal velocities can be eliminated from (2.1) and (2.2) to provide the following equation for $\tilde{v}_r$:

$$\frac{\mathrm{d}}{\mathrm{d}r}\left[\frac{r}{n^2+k^2r^2}\frac{\mathrm{d}}{\mathrm{d}r}(r\tilde{v}_r)\right] - \tilde{v}_r - \frac{r\tilde{v}_r}{U-c}\frac{\mathrm{d}}{\mathrm{d}r}\left[\frac{rU'}{n^2+k^2r^2}\right] = 0. \tag{2.3}$$

It should be noted that the form in which this equation is written here is crucial while deriving the subsequent general results for arbitrary n. If, for example, the derivatives in the above equation are expanded at this stage, then the subsequent integral manipulations become very difficult for arbitrary n and hence the previous study of Kumaran (1996) was restricted to axisymmetric ($n = 0$) and 'highly non-axisymmetric' ($n \gg k$) disturbances. The equations governing both axisymmetric disturbances ($n = 0$) and 'highly non-axisymmetric' disturbances ($n \gg k$) of Kumaran (1996) are special cases of (2.3).

The dynamics of the flexible wall is represented by the normal displacement field, u, which is the displacement of the material points in the wall medium from their steady-state positions due to velocity fluctuations. In the linear stability theory, the displacement field also has a normal mode form $u = \tilde{u}\exp[\mathrm{i}k(x-ct) + \mathrm{i}n\theta]$. Note that u is used for the displacement in the wall, and $\tilde{v}_i$ is used for the velocity field in the fluid. For small displacements, the normal stress is a linear function of the displacement field. The constitutive relation considered here is of the form (Kumaran 1996; Yeo 1994; Yeo & Dowling 1987)

$$\tilde{\sigma} = -(E - k^2c^2I - \mathrm{i}kcD)\tilde{u}, \tag{2.4}$$

where E, I and D are the positive constants associated with the elasticity, inertia and dissipation in the wall. These quantities are in general functions of k, n, c and the wall properties. The wall models used by Carpenter and co-workers (see for example, Davies & Carpenter 1997) can be written in the above form with E being a function of k and n. The ensuing generalizations are applicable for k and n dependent E, D and I as long as these quantities are stipulated to be positive. The above form for the normal stress was derived by Yeo & Dowling (1987) for a passive compliant wall using a variational Lagrangian formulation of the wall dynamics. The boundary conditions at the interface between the wall and the fluid in the inviscid limit are the continuity of velocity and normal stress:

$$-\mathrm{i}kc\tilde{u} = \tilde{v}_r, \quad \tilde{\sigma} = -\tilde{p} = (U-c)\tilde{v}_x + \tilde{v}_rU'/(\mathrm{i}k). \tag{2.5}$$

The term $(\tilde{v}_r{*}\mathrm{d}_r\tilde{v}_r)|_{r=1}$ (the superscript $*$ denotes the complex conjugate) is required as a boundary condition in the subsequent analysis, and this term can be evaluated to be

$$(\tilde{v}_r^*\mathrm{d}_r\tilde{v}_r)_{r=1} = \left[-1 - \frac{U'_w}{c} + \frac{\bar{E} - k^2c^2\bar{I} - \mathrm{i}kc\bar{D}}{c^2}\right](\tilde{v}_r\tilde{v}_r^*)|_{r=1}. \tag{2.6}$$

Here, $\{\bar{E},\bar{I},\bar{D}\} = \{E,I,D\}(k^2+n^2)/k^2$ and $\bar{E}$, $\bar{I}$ and $\bar{D}$ are positive constants. The methods used here for obtaining the general results are similar to those used in the previous studies (Howard & Gupta 1962; Maslowe 1974; Yeo & Dowling 1987; and Kumaran 1996), and therefore only the gist of the derivations is provided here.

Equivalent of the Rayleigh theorem

This is derived by multiplying (2.3) by $r\tilde{v}_r^*$ and integrating from $r=0$ to $r=1$. The resulting equation is multiplied by c and the imaginary part of this equation is

$$c_i \int_0^1 \left[\frac{r}{n^2+k^2} |\mathrm{d}_r(rv_r)|^2 + r|\tilde{v}_r|^2 + \frac{r^2|\tilde{v}_r|^2}{|U-c|^2}(\mathscr{G}'U) \right] \mathrm{d}r = -\frac{|\tilde{v}_r|^2}{n^2+k^2} \left[\frac{\bar{E}c_i + k^2|c|^2\bar{I}c_i + k|c|^2\bar{D}}{|c|^2} \right], \tag{2.7}$$

where $\mathscr{G}(r)$ is defined as $\mathscr{G}(r) = rU'(r)/(n^2+k^2r^2)$ and $\mathscr{G}' \equiv \mathrm{d}_r\mathscr{G}$. In the above equation we have used the expression for $\tilde{v}_r^*\mathrm{d}_r\tilde{v}_r$ from (2.6). For unstable modes ($c_i > 0$), the right-hand side of (2.7) is negative because $\bar{E},\bar{I},\bar{D}$ are positive quantities, and $k \geqslant 0$. The left-hand side of (2.7) can be negative only if $U\mathscr{G}'$ is negative at some point in the flow. This provides the equivalent of the Rayleigh inflection point theorem to flow in a flexible tube:

PROPOSITION 1. *For an inviscid flow in a flexible tube with $U_w = 0$, an unstable mode can exist only if $U\mathscr{G}' < 0$ somewhere in the flow, where $\mathscr{G}(r) = rU'(r)/(n^2+k^2r^2)$.*

The following corollaries can be inferred from (2.7).

COROLLARY 1. *For an inviscid flow in a flexible tube with $U_w = 0$ and $U\mathscr{G}' > 0$, all modes are neutrally stable if the wall is non-dissipative ($D = 0$).*

COROLLARY 2. *For an inviscid flow in a flexible tube with $U_w = 0$ and $U\mathscr{G}' > 0$, all modes are damped if the wall is dissipative ($D > 0$).*

Proposition 1 of this paper is a generalization of Propositions 1 and 6 of Kumaran (1996). A similar proposition for flow through rigid tubes was derived by Maslowe (1974).

Equivalent of the Fjørtoft theorem

Equation (2.3) is multiplied by $(r\tilde{v}_r^*)$, and the resulting equation is subtracted from its complex conjugate and integrated from $r=0$ to $r=1$. The integral occurring in the resulting equation is evaluated using (2.6) to give

$$-\frac{2\mathrm{i}}{(n^2+k^2)} \left[\frac{\bar{E}c_rc_i + c_rk|c|^2\bar{D}}{|c|^4} - \frac{U_w'c_i}{|c|^2} \right] (\tilde{v}_r\tilde{v}_r^*)_{(r=1)} = 2\mathrm{i}c_i \int_0^1 \mathrm{d}r \frac{r^2|\tilde{v}_r|^2}{|U-c|^2} \frac{\mathrm{d}}{\mathrm{d}r} \left[\frac{rU'}{n^2+k^2r^2} \right]. \tag{2.8}$$

It is necessary to specify further additional conditions to derive the desired results. First, consider $U_w' = -|U_w'| < 0$ and $c_r > 0$ (downstream-travelling waves). In this case, the above equation reduces to

$$-\frac{1}{(n^2+k^2)} \left[\frac{\bar{E}c_rc_i + c_rk|c|^2\bar{D}}{|c|^4} + \frac{|U_w'|c_i}{|c|^2} \right] (\tilde{v}_r\tilde{v}_r^*)_{(r=1)} = c_i \int_0^1 \mathrm{d}r \frac{r^2|\tilde{v}_r|^2}{|U-c|^2} \frac{\mathrm{d}}{\mathrm{d}r}\mathscr{G}(r), \tag{2.9}$$

where $\mathscr{G}(r) = rU'(r)/(n^2+k^2r^2)$. From the above equation, the necessary condition for unstable perturbations ($c_i > 0$) is $\mathscr{G}'(r) < 0$ somewhere in the flow. This is because the left-hand side is always negative and in order to satisfy the equality, $\mathscr{G}'(r)$ should be less than zero somewhere in the flow. Similarly, for the case when $c_r < 0$ and $U_w' > 0$, it can be easily shown that $\mathscr{G}'(r) > 0$ somewhere in the flow for unstable oscillations to exist. This gives the equivalent of the Fjørtoft theorem, and a generalization of Propositions 2 and 7 of Kumaran (1996):

PROPOSITION 2. *For an inviscid flow in a flexible tube with* $U_w = 0$ *and* $U_w' \leqslant 0$ ($U_w' \geqslant 0$), *an unstable mode with* $c_r \geqslant 0$ ($c_r \leqslant 0$) *can exist only if* $\mathscr{G}'(r) < 0$ ($\mathscr{G}'(r) > 0$) *somewhere in the flow, where* $\mathscr{G}(r) = rU'(r)/(n^2 + k^2r^2)$.

The following corollaries can be derived on inspecting the equation (2.9).

COROLLARY 1. *For an inviscid flow in a flexible tube with* $U_w = 0$ *and* $U_w' \leqslant 0$ ($U_w' \geqslant 0$), *and* $\mathscr{G}'(r) > 0$ ($\mathscr{G}'(r) < 0$), *all modes with* $c_r > 0$ ($c_r < 0$) *are neutrally stable if the wall is non-dissipative* ($D = 0$), *where* $\mathscr{G}'(r) = rU'(r)/(n^2 + k^2r^2)$.

COROLLARY 2. *For an inviscid flow in a flexible tube with* $U_w = 0$ *and* $U_w' \leqslant 0$ ($U_w' \geqslant 0$), *and* $\mathscr{G}'(r) > 0$ ($\mathscr{G}'(r) < 0$), *all modes with* $c_r > 0$ ($c_r < 0$) *are damped if the wall is dissipative* ($D > 0$), *where* $\mathscr{G}'(r) = rU'(r)/(n^2 + k^2r^2)$.

A similar proposition for flow through rigid tubes was derived by Maslowe (1974). For a parabolic flow in a flexible tube, the laminar flow velocity profile $U(r) = (1-r^2)$, and the criterion $\mathscr{G}'(r) < 0$ yields

$$\mathscr{G}'(r) = \frac{-4rn^2}{(n^2 + k^2r^2)^2} < 0. \tag{2.10}$$

For axisymmetric disturbances, $n = 0$, and the criterion $\mathscr{G}'(r) < 0$ is *not* satisfied. This implies that the parabolic flow in a flexible tube is stable in the inviscid limit to axisymmetric disturbances. However, for any $n > 0$, the criterion $\mathscr{G}'(r) < 0$ is satisfied, and the present result suggests that the parabolic flow in a flexible tube could be unstable in the inviscid limit to non-axisymmetric perturbations of any non-zero azimuthal wavenumber. It is also instructive to obtain the necessary condition for instability in flow through rigid tubes from (2.9). For the case of flow in rigid tubes, the left-hand side of (2.9) is identically zero because the normal velocity at the wall is zero for flow in a rigid tube. Thus the right-hand side of (2.9) is zero:

$$c_i \int_0^1 \mathrm{d}r \frac{r^2|\tilde{v}_r|^2}{|U-c|^2} \frac{\mathrm{d}}{\mathrm{d}r}\mathscr{G}(r) = 0. \tag{2.11}$$

For unstable modes ($c_i > 0$), for the above integral to be zero, the function $\mathscr{G}'(r)$ should change its sign from positive to negative somewhere in the flow. This result is in agreement with the result of Howard & Gupta (1962), who have derived general results for inviscid flow through rigid concentric cylinders. For the case of fully-developed parabolic flow in a rigid tube, the expression for $\mathscr{G}'(r)$ is given in (2.10), and it can be seen that $\mathscr{G}'(r) \leqslant 0$, and it never changes its sign in the flow. Thus, the parabolic flow in a rigid tube is stable in the inviscid limit to all types of small disturbances.

Bounds for c_r

Consider the function $g(r) \equiv r\tilde{v}_r/(U-c)$. Using the definition of g the expression for g^*g' can be derived from (2.6). The governing equation (2.3) can be expressed in

terms of $g(r)$ and the resulting equation is multiplied by g^*, the complex conjugate of g, and integrated from $r = 0$ to $r = 1$:

$$\int_0^1 (U-c)^2 \Phi \, \mathrm{d}r = \frac{|\tilde{v}_r|^2}{|c|^2(n^2+k^2)}(\bar{E} - k^2c^2\bar{I} - \mathrm{i}kc\bar{D}), \tag{2.12}$$

where $\Phi = [r|g'|^2/(n^2+k^2r^2) + |g|^2/r]$. It is sufficient to note that Φ is a positive, real function. Consider the imaginary part of the above equation:

$$2c_i \int_0^1 (U-c_r)\Phi \, \mathrm{d}r = \frac{c_r}{|c|^2(n^2+k^2)}(2k^2\bar{I}c_i + k\bar{D}). \tag{2.13}$$

From (2.13) certain conclusions can be made regarding the range of the real part of the wave speed c_r, for potentially unstable modes ($c_i > 0$). It is convenient to define the following quantities: $U_L = \min[U_{\min}, 0]$, $U_U = \max[U_{\max}, 0]$, $U_{\min} = \min_r[U(r)]$, $U_{\max} = \max_r[U(r)]$. The following Proposition can easily be proved on inspecting (2.13):

PROPOSITION 3. *For an inviscid flow in a flexible tube with $U_w = 0$, all unstable (axisymmetric and non-axisymmetric) modes have $U_L < c_r < U_U$, where U_L and U_U are as defined before.*

This Proposition is an extension of Proposition 1 of Yeo & Dowling (1987) to the case of inviscid flow in a flexible tube. In Kumaran (1996), bounds were derived for c_r for axisymmetric and highly non-axisymmetric disturbances. The present result (Proposition 3) does not reduce to the results of Kumaran (1996) because the Proposition 3 of the present work is a much stronger result on the bounds of c_r than the Propositions 3 and 8 of Kumaran (1996). Moreover, in contrast to Proposition 3 of the present work, the Proposition 8 in Kumaran (1996) for highly non-axisymmetric modes is inconclusive for $n = 1$, as the bound becomes singular at $n = 1$.

Bounds on $|c|$

Equation (2.12) is multiplied by c^*, the complex conjugate of the wave speed, and the imaginary part of the resulting equation is taken:

$$c_i \int_0^1 (|c|^2 - U^2)\Phi \, \mathrm{d}r = -\frac{[\bar{E}c_i + k|c|^2\bar{I}c_i + k|c|^2\bar{D}]}{|c|^2(n^2+k^2)}. \tag{2.14}$$

The right-hand side of the above equation is always negative for unstable modes ($c_i > 0$), so the integral in the left-hand side should be less than zero. Since Φ is a positive and real function, for the above equality to hold, we require $|c|^2 < \max(U^2)$.

PROPOSITION 4. *For an inviscid flow in a flexible tube with $U_w = 0$, all unstable (axisymmetric and non-axisymmetric) modes have $|c|^2 < \max(U^2)$.*

Equivalent of the Howard semi-circle theorem

The semi-circle theorem provides a bound on the phase velocity c for unstable modes in the complex-c plane. A positive real function A is defined as $A = |\tilde{v}_r|^2/[|c|^2(n^2+k^2)]$. Equation (2.12), expressed in terms of the function A, is

$$\int_0^1 (U-c)^2 \Phi \, \mathrm{d}r = A[\bar{E} - k^2c^2\bar{I} - \mathrm{i}kc\bar{D}]. \tag{2.15}$$

The real and imaginary parts of (2.15) are

$$\int_0^1 [(U-c_r)^2 - c_i^2]\Phi \,\mathrm{d}r = A[\bar{E} - k^2(c_r^2 - c_i^2)\bar{I} + kc_i\bar{D}], \tag{2.16}$$

$$2c_i \int_0^1 (U-c_r)\Phi \,\mathrm{d}r = c_r kA[2kc_i\bar{I} + \bar{D}]. \tag{2.17}$$

Since

$$\int_0^1 \mathrm{d}r\ (U-U_{\min})(U-U_{\max})\Phi < 0, \tag{2.18}$$

for $U_{\min} = \min[U(r)]$ and $U_{\max} = \max[U(r)]$, the following expressions can be derived using (2.16) and (2.17):

$$\int_0^1 U^2\Phi \,\mathrm{d}r = \int_0^1 |c|^2\Phi \,\mathrm{d}r + A\left[\bar{I}k^2c_r + \bar{E} + \frac{k\bar{D}|c|^2}{c_i}\right], \tag{2.19}$$

$$\int_0^1 U\Phi \,\mathrm{d}r = \int_0^1 c_r\Phi \,\mathrm{d}r + A\left[c_rk^2\bar{I} + \frac{kc_r\bar{D}}{2c_i}\right]. \tag{2.20}$$

The above two equations are very similar to the equations (3.20) and (3.21) of Yeo & Dowling (1987), and the arguments used by Yeo & Dowling (1987) to extend the Howard semi-circle theorem for the planar case exactly carries over to the axisymmetric geometry considered here. Therefore, we do not repeat the arguments here and refer the reader to Shankar (1999) for more details. The extension of the semi-circle theorem for the case of inviscid flow in a flexible tube is stated in the following Proposition.

PROPOSITION 5. *For an inviscid flow in a flexible tube with $U_w = 0$, all unstable modes must satisfy*

$$\left[c_r - \tfrac{1}{2}(U_U + U_L)\right]^2 + c_i^2 < \left[\tfrac{1}{2}(U_U - U_L)\right]^2,$$

where U_L and U_U are as defined before.

The bounds for the wave speed derived in this paper (Propositions 3, 4 and 5) do not assume any restriction on the nature of the mean velocity profile, apart from requiring that the mean velocity at the wall is zero. In the analysis of Kumaran (1996), certain bounds for the real part of the wave speed and $|c|^2$ were derived for velocity profiles with $UU'_w < 0$. This condition on the velocity profile is restrictive, since biological flows due to oscillatory pressure gradients involve backflow in certain regions and do not follow this inequality. The Propositions 3, 4 and 5 of the present work are stronger than the equivalent propositions derived in Kumaran (1996) in the axisymmetric and highly non-axisymmetric limits.

Equivalent of the Høiland theorem

The theorem of Høiland (Drazin & Reid 1981), which places restrictions on the imaginary part of the phase velocity, can be extended to the case of inviscid flow through a flexible tube. The function $f(r)$ is defined as $f(r) = r\tilde{v}_r/(U-c)^{1/2}$. The governing equation (2.3) after being expressed in terms of f, is multiplied by f^* and integrated from $r = 0$ to $r = 1$. This equation contains the expression $(f^*\mathrm{d}_r f)_{r=1}$ which can be evaluated from the expression for $\tilde{v}_r^*\mathrm{d}_r\tilde{v}_r$ (see (2.6)), and the imaginary part of

the resulting equation is multiplied by c_i to give

$$\int_0^1 \mathrm{d}r c_i^2 \left[\frac{r|\mathrm{d}_r f|^2}{n^2+k^2r^2}\right] + \int_0^1 \mathrm{d}r|f|^2 \left\{\frac{c_i^2}{r} - \frac{r}{n^2+k^2r^2}\left[\frac{U'c_i}{2|U-c|}\right]^2\right\} = -\frac{|f|_1^2}{|c|^2}\frac{[\bar{E}c_i^2 + |c|^2\bar{I}c_i^2 + k|c|^2\bar{D}c_i]}{n^2+k^2}. \tag{2.21}$$

The first term on the left-hand side of (2.21) is always positive for unstable modes $c_i > 0$. The term on the right-hand side of (2.21) is always negative. Thus, the second term on the left-hand side of (2.21) has to be negative. This places the following restriction on c_i after noting that $c_i^2 \leqslant |U-c|^2$.

PROPOSITION 6. *For an inviscid flow in a flexible-walled tube with $U_w = 0$, all unstable waves satisfy*

$$c_i < \max\left[\frac{r^2(U')^2}{4(n^2+k^2r^2)}\right]^{1/2}. \tag{2.22}$$

This completes the generalization of classical theorems of hydrodynamic stability to the case of arbitrary disturbances to flow in a flexible tube.

3. Stability of Hagen–Poiseuille flow

Propositions 1 and 2 of the previous section suggest that the parabolic flow in a flexible tube could be unstable to non-axisymmetric disturbances. The rest of this paper is concerned with the stability analysis of the Poiseuille flow in a flexible tube to non-axisymmetric disturbances. The system we consider is the flow of an incompressible Newtonian fluid of density ρ and viscosity η in a tube of radius R, which is surrounded by a visco-elastic medium of density ρ, viscosity η_w and coefficient of elasticity G in the annular space $R < r < HR$. In the present analysis, the density of the fluid and the wall material is assumed to be the same for simplicity. The present formulation can be extended in a straightforward fashion to the case where the densities are different. In the limit of high Reynolds number, lengths are scaled by the radius of the tube R, velocities by $(G/\rho)^{1/2}$ and time by $(\rho R^2/G)^{1/2}$. The mean flow velocity profile whose stability is of interest in this study is the Hagen–Poiseuille flow which is represented in non-dimensional form as

$$\bar{v}_x = \Gamma U = \Gamma(1-r^2). \tag{3.1}$$

Here, $\Gamma = (\rho U_{max}^2/G)^{1/2}$ is the dimensionless maximum velocity of the base flow, and U_{max} is the maximum fluid velocity of the Hagen–Poiseuille flow. The scaled Navier–Stokes equations governing the motion in the fluid are

$$\partial_i v_i = 0, \tag{3.2}$$

$$\partial_i v_j + v_j \partial_j v_i = -\partial_i p + \Gamma Re^{-1}\partial_j^2 v_i, \tag{3.3}$$

where $\partial_t = (\partial/\partial t)$ and $\partial_i = (\partial/\partial x_i)$, $Re = (\rho U_{max} R/\eta)$ is the Reynolds number, and repeated indices imply a summation over that index. The pressure in the fluid is non-dimensionalised by the shear modulus G. The stress tensor in the fluid is

$$\tau_{ij} = -p\delta_{ij} + Re^{-1}\Gamma(\partial_i v_j + \partial_j v_i). \tag{3.4}$$

The flexible wall is assumed to be a viscoelastic solid continuum, and the dynamics of the wall motion is described by the governing equations for an incompressible elastic

material (Landau & Lifshitz 1989) modified to include viscous stresses. The dynamics of the wall is represented by a displacement field u_i which describes the displacement of the material points in the wall medium from their steady-state positions due to velocity perturbations. The wall material is assumed to be incompressible, and the mass conservation equation is

$$\partial_i u_i = 0, \tag{3.5}$$

and the momentum balance equation is

$$\partial_t^2 u_i = -\partial_i p + \partial_j^2 u_i + Re^{-1} \Gamma \eta_r \partial_j^2 v_i, \tag{3.6}$$

where $\eta_r = \eta_w/\eta$ is the ratio of the viscosity of the wall material and the fluid. The stress tensor in the wall medium is given by

$$\sigma_{ij} = -p\delta_{ij} + (\partial_i u_j + \partial_j u_i) + Re^{-1} \Gamma \eta_r (\partial_i v_j + \partial_j v_i). \tag{3.7}$$

The second term on the right-hand side of (3.6) has a coefficient of unity because the momentum equation has been scaled with G, the shear modulus of the wall medium. In (3.6), $v_i = \partial_t u_i$ is the velocity in the wall material. The above form for the momentum equation and the stress tensor, incorporating frequency-independent coefficients of elasticity and viscosity, was derived in Harden, Pleiner & Pincus (1991) to describe surface fluctuations on polymer gels, and has been used in the previous stability analyses of Kumaran (1995*a*, *b*, 1998*a*, *b*). Two assumptions have been made in the above constitutive relation. First, the linearity assumption when relating the stress to the strain rate and secondly the assumption of frequency-independent storage modulus and viscosity. Experimental studies have reported that the storage modulus for polymer gels does have a constant 'plateau value' for a wide range of frequencies 10^{-2} to 10^3 s^{-1} (Tong & Liu 1993), and the assumption regarding the frequency-independent elasticity is well-founded. For the viscosity, which is related to the loss modulus, we have made the simplest assumption where η_w is considered to be frequency-independent. However, the neutral stability curves obtained in the present analysis can easily be extended to a wall material with frequency-dependent viscosity. For a system with viscosity $\eta_r'(\omega)$ dependent on the frequency ω, the critical value of $\eta_{rc}'(\omega)$ for neutrally stable modes is related to the critical value η_{rc} determined in the present analysis for frequency-independent viscosity by the relation $\eta_{rc}'(\omega_c) = \eta_{rc}$ where ω_c is the frequency of the neutrally stable modes obtained in the present analysis. The wall medium is assumed to be fixed at $r = H$ and the displacement field satisfies $u_i = 0$ for $i = r, \theta, x$. The boundary conditions at the interface between the fluid and the wall are the continuity of velocity and stress:

$$v_i = \partial_t u_i, \quad \sigma_{ij} = \tau_{ij}. \tag{3.8}$$

In the linear stability analysis, small-amplitude non-axisymmetric perturbations in the form of Fourier modes are imposed on the fluid velocity field and the wall displacement field:

$$v_i = \tilde{v}_i \exp[\mathrm{i}k(x - ct) + \mathrm{i}n\theta], \quad u_i = \tilde{u}_i \exp[\mathrm{i}k(x - ct) + \mathrm{i}n\theta], \tag{3.9}$$

where k is the wavenumber along the axial direction, n is the wavenumber in the azimuthal direction and c is the wave speed of perturbations and the index $i = r, \theta, x$. The wavenumber k and n are real for a temporal stability analysis, and $c = c_r + \mathrm{i}c_i$ is a complex quantity with $c_i > 0$ for unstable modes. On substituting the above form for perturbations into the governing Navier–Stokes equations for the fluid, the following

set of equations is obtained:

$$(\mathrm{d}_r + r^{-1})\tilde{v}_r + \mathrm{i}nr^{-1}\tilde{v}_\theta + \mathrm{i}k\tilde{v}_x = 0, \tag{3.10}$$

$$\mathrm{i}k(\Gamma U - c)\tilde{v}_r = Re^{-1}\Gamma[(\mathrm{d}_r^2 + r^{-1}\mathrm{d}_r - r^2) - (k^2 + n^2r^{-2})]\tilde{v}_r - \mathrm{d}_r\tilde{p} - 2\mathrm{i}nRe^{-1}\Gamma r^{-2}\tilde{v}_\theta, \tag{3.11}$$

$$\mathrm{i}k(\Gamma U - c)\tilde{v}_\theta = Re^{-1}\Gamma[(\mathrm{d}_r^2 + r^{-1}\mathrm{d}_r - r^{-2}) - (k^2 + n^2r^{-2})]\tilde{v}_\theta - r^{-1}\mathrm{i}n\tilde{p} + 2Re^{-1}\Gamma r^{-2}\mathrm{i}n\tilde{v}_r, \tag{3.12}$$

$$\mathrm{i}k(\Gamma U - c)\tilde{v}_x + \Gamma U'\tilde{v}_r = -\mathrm{i}k\tilde{p} + Re^{-1}\Gamma[\mathrm{d}_r^2 + r^{-1}\mathrm{d}_r - (n^2r^{-2} + k^2)]\tilde{v}_x. \tag{3.13}$$

The following governing equations for the displacement field $\tilde{u}_i$ in the wall material are obtained by inserting the perturbation to the wall displacement field into (3.5) and (3.6):

$$(\mathrm{d}_r + r^{-1})\tilde{u}_r + \mathrm{i}nr^{-1}\tilde{u}_\theta + \mathrm{i}k\tilde{u}_x = 0, \tag{3.14}$$

$$-k^2c^2\tilde{u}_r = -\mathrm{d}_r\tilde{p}_g + (1 - \mathrm{i}kcRe^{-1}\eta_r\Gamma)[\mathrm{d}_r^2 + r^{-1}\mathrm{d}_r - r^{-2}(1+n^2) - k^2]\tilde{u}_r - 2r^{-2}\mathrm{i}n\tilde{u}_\theta, \tag{3.15}$$

$$-k^2c^2\tilde{u}_x = -\mathrm{i}k\tilde{p}_g + (1 - \mathrm{i}kcRe^{-1}\eta_r\Gamma)[\mathrm{d}_r^2 + r^{-1}\mathrm{d}_r - r^{-2}n^2 - k^2]\tilde{u}_x, \tag{3.16}$$

$$-k^2c^2\tilde{u}_\theta = -r^{-1}\mathrm{i}n\tilde{p}_g + (1 - \mathrm{i}kcRe^{-1}\eta_r\Gamma)[\mathrm{d}_r^2 + r^{-1}\mathrm{d}_r - r^{-2}(1+n^2) - k^2]\tilde{u}_x + 2r^{-2}\mathrm{i}n\tilde{u}_r. \tag{3.17}$$

The boundary conditions for the fluid at the centre of the tube ($r = 0$) are the kinematic conditions which state that the fluid velocity and pressure should be bounded and continuous (Batchelor & Gill 1962). The boundary conditions at $r = 0$ are

$$\left.\begin{array}{ll} \tilde{v}_z(0) = \tilde{p}(0) = 0 & \text{for } n \neq 0, \\ \tilde{v}_z(0) \text{ and } \tilde{p}(0) \text{ finite} & \text{for } n = 0, \end{array}\right\} \tag{3.18}$$

$$\left.\begin{array}{ll} \tilde{v}_r(0) = \tilde{v}_\theta(0) = 0 & \text{for } n \neq 1, \\ \tilde{v}_r(0) + \mathrm{i}\tilde{v}_\theta(0) = 0 & \text{for } n = 1. \end{array}\right\} \tag{3.19}$$

The boundary conditions at the fluid–wall interface are the continuity of velocities and stress applied at the perturbed interface. In a linear stability analysis, the dynamical variables are expanded in a series about the unperturbed interface ($r = 1$) and the terms linear in the perturbations to the velocity and displacement fields are retained to obtain the following conditions at $r = 1$:

$$\tilde{v}_r = -\mathrm{i}kc\tilde{u}_r, \quad \tilde{v}_\theta = -\mathrm{i}kc\tilde{u}_\theta, \quad \tilde{v}_x - 2\Gamma\tilde{u}_r = -\mathrm{i}kc\tilde{u}_x, \tag{3.20}$$

$$\tilde{\tau}_{rr} = \tilde{\sigma}_{rr}, \quad \tilde{\tau}_{xr} = \tilde{\sigma}_{xr}, \quad \tilde{\tau}_{r\theta} = \tilde{\sigma}_{r\theta}. \tag{3.21}$$

The second term on the left-hand side of the third equation in (3.20) (the boundary condition for the tangential velocity), which represents the variation in the mean flow velocity at the surface due to surface displacement (Kumaran 1995*a*, *b*), is due to the discontinuity of strain rate across the interface in the base state. However, the stresses in the base state are continuous and no such additional terms appear in the stress continuity conditions. The boundary conditions at the surface $r = H$ are the zero displacement conditions ($\tilde{u}_r = \tilde{u}_x = \tilde{u}_\theta = 0$). The equations (3.10)–(3.17) can be solved numerically to obtain the eigenfunctions in the fluid and wall media. However, these equations are nonlinear in the wave speed and it is necessary to have a good initial guess in order to obtain numerical solutions. To provide this initial guess, and to determine the structure of the solutions at high Reynolds number, an asymptotic analysis is carried out in this limit.

3.1. *High Reynolds number asymptotic analysis*

In this subsection, an asymptotic analysis of the stability equations is performed in the limit of high Reynolds number. In the leading approximation, the terms of $O(Re^{-1})$ are neglected in the fluid and wall governing equations. The perturbation velocity $\tilde{v}_r$ is determined by solving the equation (2.3). The inviscid governing equation (2.3) is non-dimensionalized according to the scales given in this section as follows:

$$\frac{\mathrm{d}}{\mathrm{d}r}\left[\frac{r}{n^2+k^2r^2}\frac{\mathrm{d}}{\mathrm{d}r}(r\tilde{v}_r)\right]-\tilde{v}_r-\frac{r\tilde{v}_r}{(U-c/\Gamma)}\frac{\mathrm{d}}{\mathrm{d}r}\left[\frac{rU'}{n^2+k^2r^2}\right]=0. \tag{3.22}$$

Proposition 3 of §2 states that for unstable modes in the inviscid limit, the wave speeds are such that they lie between the maximum and the minimum of the base flow velocity profile. For neutral modes (c is real), the point where the wave speed is equal to the mean fluid velocity is a regular singular point, called the 'critical point'. Near this singular point, viscous effects become important and this results in a critical layer of thickness $O(Re^{-1/3})$ (Drazin & Reid 1981, Chap. 4). In the limit of high Re, there is another region near the wall of thickness $O(Re^{-1/2})$ where viscous effects become important. In the following analysis, the critical and wall layers are assumed to be well separated.

There are two linearly independent solutions of the equation (3.22) near the regular singular point using a Frobenius expansion about r_c (Drazin & Reid 1981, Chap. 4):

$$\phi_1(r)=(r-r_c)P_1(r), \tag{3.23}$$

$$\phi_2(r)=P_2(r)+\phi_1(r)\log(r-r_c), \tag{3.24}$$

where $P_1(r)$ and $P_2(r)$ are polynomials in $(r-r_c)$ whose coefficients are obtained using symbolic computation. $P_1(r)$ is analytic at r_c and hence $\phi_1(r)$ is also analytic at the critical point, but $\phi_2(r)$ has a logarithmic singular point at r_c. This logarithmic term is multi-valued and there is an ambiguity about the correct branch of the logarithm in the evaluation of the inviscid solution. This ambiguity cannot be resolved using the inviscid theory, and it is necessary to obtain the viscous solution in the critical layer. The correct branch of the logarithm is determined by matching the inviscid solution in the outer region and the viscous solution in the critical layer. The scaling analysis near the critical layer for non-axisymmetric disturbances, where there is an additional velocity component $\tilde{v}_\theta$, can be carried out using methods similar to the classic work of Lin (1945). The details of this analysis are provided in Shankar (1999). This analysis shows that the correct branch of logarithm for $r<r_c$ is

$$\log(r-r_c)=\log|r-r_c|+\mathrm{i}\pi, \tag{3.25}$$

if $\log(r-r_c)=\log|r-r_c|$ for $r>r_c$. Using the analytical expressions for the two linearly independent solutions near the critical point as initial conditions, the equation (3.22) is integrated numerically using a fourth-order Runge–Kutta method. The ranges for the numerical integration are from $r=r_c+\epsilon$ to $r=1$ and from $r=r_c-\epsilon$ to $r=0$ where ϵ is a small quantity $\sim 10^{-4}$. The governing equations for the wall material in the inviscid limit are obtained by neglecting the terms of $O(Re^{-1})$ in the equations (3.14)–(3.17). These equations were solved using a numerical fourth-order Runge–Kutta integration procedure. The boundary conditions at the wall $r=H$ are $\tilde{u}_r=\tilde{u}_\theta=\tilde{u}_x=0$ at this point. The general solution can then be written as a linear combination of the three eigenfunctions in the wall medium. The boundary conditions

at $r = 1$ for the inviscid flow are

$$\tilde{\sigma}_{r\theta} = 0, \quad \tilde{\sigma}_{rx} = 0, \quad \tilde{\tau}_{rr} = \tilde{\sigma}_{rr}, \quad \tilde{v}_r = -\mathrm{i}kc\tilde{u}_r. \tag{3.26}$$

Note that the shear stresses in the fluid ($\tilde{\tau}_{xr}$, $\tilde{\tau}_{r\theta}$) are set to zero in the inviscid approximation, and there are no conditions on the tangential velocity ($\tilde{v}_x$, $\tilde{v}_\theta$). The above conditions, along with the kinematic conditions at the centre of the tube (3.18), (3.19) are used to assemble a 5×5 characteristic matrix, and the determinant of the characteristic matrix is set to zero in order to obtain the wave speed c. It was found convenient to fix c_r/Γ such that it lies between 0 and 1 (i.e. the neutral modes are singular) and treat Γ as the eigenvalue. Thus, for a given set of k, H, n, Γ is calculated for a known value of (c_r/Γ). The characteristic equation admits multiple solutions for Γ for a fixed value of c_r/Γ.

In order to verify that the neutral mode does become unstable for a small change in the velocity, the following numerical procedure was adopted. Since $c_i > 0$ for unstable modes, the governing equation (3.22) is regular even if $0 < c_r/\Gamma < 1$. A series solution consistent with the boundary conditions (3.18), (3.19) was obtained for the velocity field near $r = 0$. Using this as an initial condition near $r = 0$, the governing equation (3.22) was numerically integrated to $r = 1$. The procedure for determining the eigenfunctions in the wall material was identical to that for the neutral modes. Using the boundary conditions at $r = 1$, namely normal velocity continuity, continuity of tangential ($\tau_{r\theta}$ and τ_{rx}) and normal stresses, a 4×4 characteristic matrix was assembled. The determinant of this matrix is set to zero in order to obtain the unknown eigenvalue. By letting Γ be very close to the neutral value, the wave speed c was calculated from the characteristic equation. It was found that c_i was indeed positive indicating that the flow is unstable in the inviscid limit. Thus, this asymptotic calculation verifies the Propositions 1 and 2 of the present work which predict that the Poiseuille flow could become unstable in the inviscid limit. It is of interest to determine whether this instability is captured by an analysis of the complete stability equations and the values of Reynolds number up to which this instability persists. This is accomplished using a numerical solution of the complete equations governing the stability in the next subsection.

3.2. *Stability at intermediate Reynolds numbers*

In this subsection, the complete equations governing the stability of the flow (3.10)–(3.17) are solved using a numerical method. For $r \to 0$, the eigenfunctions are expanded in a Frobenius series in r. This series solution is extended up to a small but finite value of r. Using these as the initial conditions, the governing stability equations are numerically integrated to the fluid–wall interface at $r = 1$. Following Garg & Rouleau (1972), it was found convenient to work with the variables $f(r) = \tilde{v}_r(r) + \mathrm{i}\tilde{v}_\theta(r)$ and $g(r) = \tilde{v}_r(r) - \mathrm{i}\tilde{v}_\theta(r)$ instead of $\tilde{v}_r$ and $\tilde{v}_\theta$. The governing equations for stability in the fluid can easily be represented in terms of these new variables. The boundary conditions in the transformed variables follow directly from (3.20), (3.21), (3.18), (3.19). A Gram–Schmidt orthonormalization procedure was implemented in order to overcome the stiff nature of the governing equations in the limit of high *Re*. The equations in the wall medium are also transformed using a similar procedure. Using the three boundary conditions at $r = H$, three linearly independent eigenfunctions can be obtained in the wall medium. There are six continuity conditions at the fluid–wall interface, namely that of normal stress, tangential stresses ($r\theta$ and rx), normal velocity, and tangential velocities (x and θ components). The eigenfunctions for the fluid velocity field and the wall displacement field were substituted in the six boundary

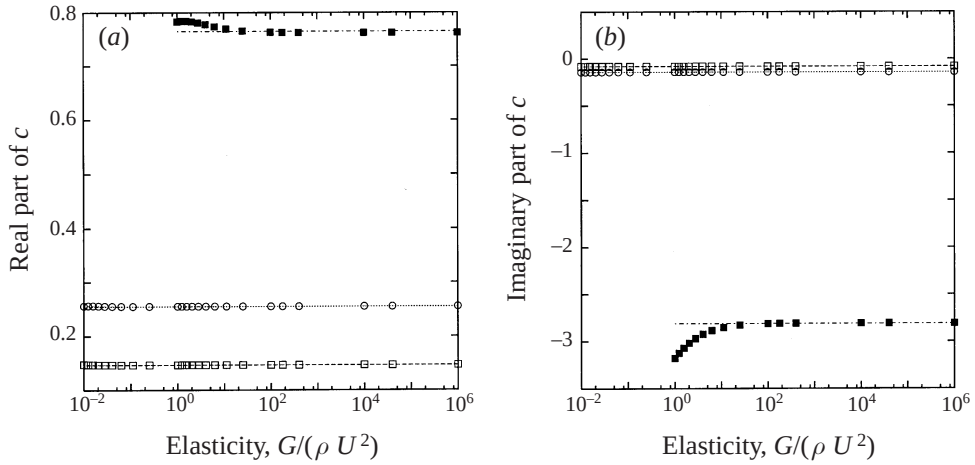

FIGURE 1. Comparison of present numerical results (symbols) with the rigid tube results of Salwen & Grosch (1972) (lines): (*a*) real part and (*b*) imaginary part of wave speed vs. $G/(\rho U_{max}^2)$ for $H = 2, k = 1, n = 1$. □, $Re = 10^4$; ○, $Re = 10^4$; ■, $Re = 10$.

conditions, and a 6×6 characteristic matrix was assembled. The determinant of this matrix is set to zero to obtain the wave speed c.

In order to validate this numerical procedure, the results obtained from this method are compared with that of Salwen & Grosch (1972) where the stability of Poiseuille flow in a rigid tube to non-axisymmetric disturbances was studied. The rigid tube limit can be recovered from the numerical procedure used in this study by considering the limit of large elasticity, i.e. $\Gamma^{-2} = G/(\rho U_{max}^2) \to \infty$. The data presented in tables 1 and 2 of Salwen & Grosch (1972) were used as initial guesses for the present numerical procedure for $\Gamma \ll 1$ and a given H. In figures 1(*a*) and 1(*b*) the flexible tube solution obtained using the numerical method of the present work is compared with the rigid tube solution of Salwen & Grosch (1972) as a function of Γ^{-2}. The flexible tube solution converges to the rigid tube solution when $G/(\rho U_{max}^2) \sim 10$. The rigid tube results can also be recovered by fixing $G/(\rho U_{max}^2)$ and considering the limit $(H - 1) \to 0$. In figures 2(*a*) and 2(*b*) the flexible tube solution is compared with the rigid tube solution as a function of $(H - 1)$. Here again, the flexible tube solutions converges to the rigid tube solution of Salwen & Grosch (1972) as $(H - 1) \to 0$ for different values of $G/(\rho U_{max}^2)$. Thus, the numerical method used in the present work is consistent with the results obtained for stability of Poiseuille flow in a rigid tube to non-axisymmetric disturbances in appropriate limits.

3.3. *Results*

Using the results obtained from the high-Re asymptotic analysis as starting guesses, the full numerical procedure outlined above was employed to continue the neutral modes to lower Re. The transition Reynolds number at which the Hagen–Poiseuille velocity profile becomes unstable depends on the following parameters: the axial wavenumber k, the azimuthal wavenumber n, the dimensionless base flow velocity Γ, the ratio of wall thickness to fluid thickness H, and the ratio of wall to fluid viscosities η_r. In figures 3(*a*) and 3(*b*) the results obtained from the inviscid calculation as outlined in § 3.1 are compared with the results obtained from the full numerical solution. The results are compared for singular inviscid neutral modes, and the wave speed c is therefore a real quantity. Figure 3(*a*) shows the comparison for the real part of

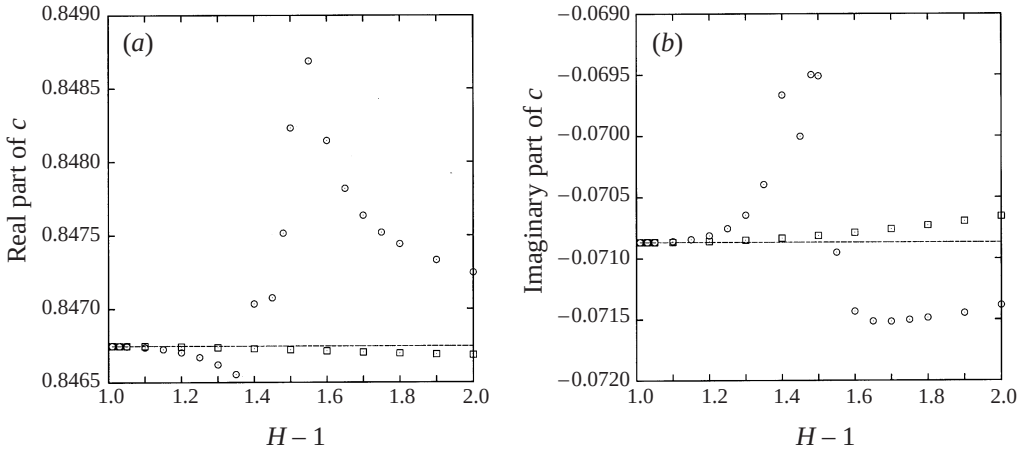

FIGURE 2. Comparison of present numerical results (symbols) with the rigid tube results of Salwen & Grosch (1972) (lines): (*a*) real part and (*b*) imaginary part of wave speed vs. $(H-1)$, for $G/(\rho U_{max}^2) = 2$ (□) and $G/(\rho U_{max}^2) = 5$ (○). $Re = 10^3, k = n = 1$.

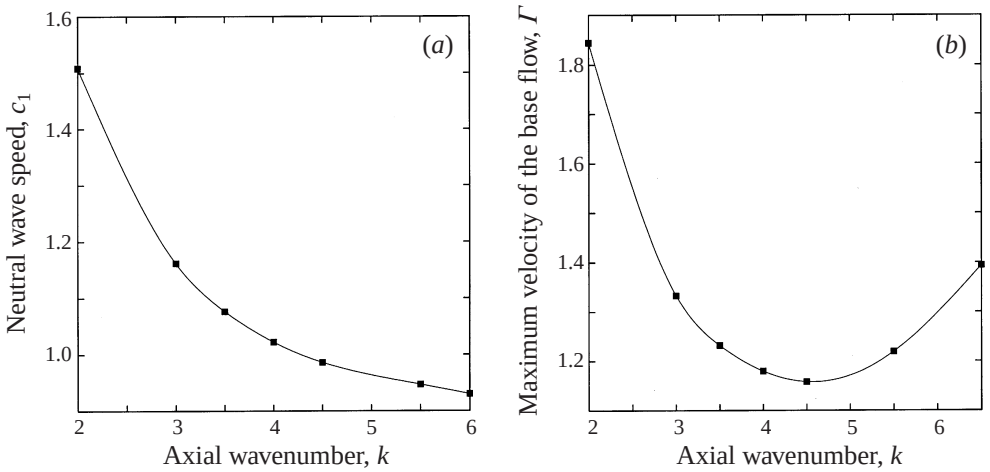

FIGURE 3. Comparison of inviscid calculation results (symbols) with the results obtained from full numerical calculation (line) for azimuthal wavenumber $n = 2$, $Re = 10^5$, $H = 2$, $\eta_r = 0$: (*a*) neutral wave speed (c_r) vs. axial wavenumber (k); (*b*) non-dimensional maximum speed of the base flow (Γ) for the neutral modes of (*a*) vs. the axial wavenumber (k).

the wave speed c_r and figure 3(*b*) shows the comparison for Γ, the corresponding non-dimensional maximum speed of the mean flow. Both these figures show that the full numerical and the inviscid results agree very well at high Reynolds numbers. In figure 4, the real part of $\tilde{v}_r$ eigenfunctions obtained from the inviscid analysis is compared with the eigenfunctions of the full numerical solution, for two different values of n and H. The eigenfunctions are normalized such that the real part of $\tilde{v}_r$ is set to 1 at $r = 1$. This figure shows that there is good agreement between the inviscid and full numerical calculations. In figure 5, the real part of $\tilde{v}_x$ eigenfunctions obtained from the full numerical analysis is plotted for $Re = 100, 1000, 5000$. The $\tilde{v}_x$ eigenfunctions are normalized such that the real part of $\tilde{v}_x$ is set to 1 at $r = 1$. This figure illustrates the emergence of sharp gradients in the $\tilde{v}_x$ velocity in the bulk of the

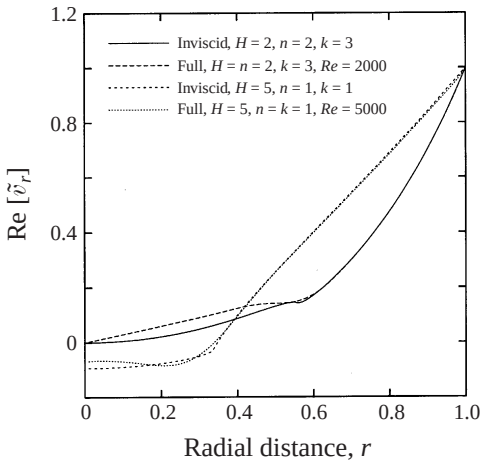

FIGURE 4. Comparison of eigenfunctions obtained from the inviscid analysis with the results of the full numerical analysis: real part of $\tilde{v}_r$ for $H = 2, n = 2, k = 3, \eta_r = 0$ and $H = 5, n = 1, k = 1, \eta_r = 0$.

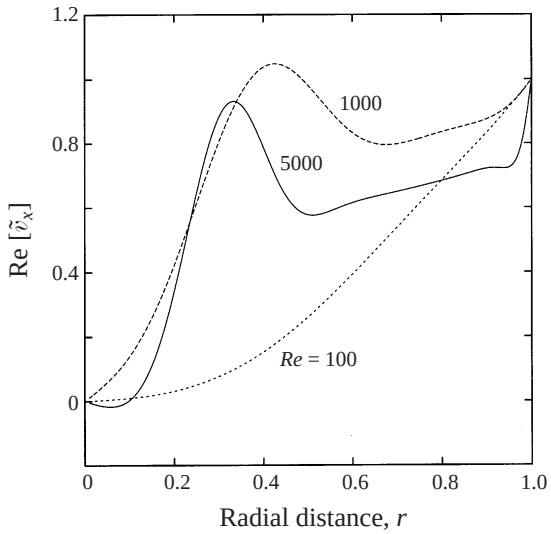

FIGURE 5. The real part of the $\tilde{v}_x$ eigenfunction obtained from the full numerical calculation showing the emergence of sharp gradients near the critical and wall layers: $H = 5$, $n = 1$, $k = 1$, $\eta_r = 0$.

flow (critical layer) and near $r = 1$ (wall layer), as the Reynolds number is increased. The critical and wall layers are clearly identifiable at $Re = 5000$, and they are well separated from each other.

A numerical continuation procedure was used to continue the asymptotic results to lower values of the Reynolds number, and the initial Reynolds number was usually set to 10^5. All the results are plotted in terms of Re vs. Σ, where $\Sigma = (\rho G R^2/\eta^2) = (Re/\Gamma)^2$ is a parameter that depends only on the material properties of the fluid and the wall, and it is independent of the flow parameters. In figure 6, the neutral stability curve is plotted in the Re vs. Σ plane for the instability obtained in the present work for $H = 2$, $n = 1$, $k = 3$ and $\eta_r = 0$. As mentioned in § 3.1, the characteristic equation of the inviscid stability problem admits multiple solutions for fixed values of H, n,

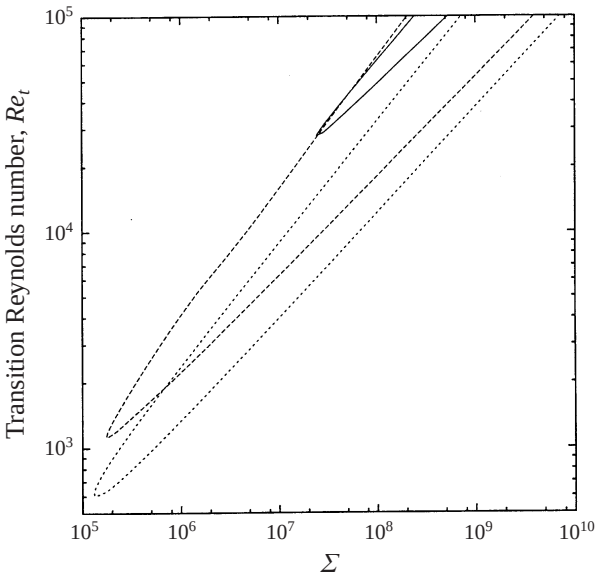

FIGURE 6. The neutral stability loops illustrating multiple solutions for $H = 2, n = 1, k = 3, \eta_r = 0$.

k and η_r. Figure 6 shows three neutral 'loops' corresponding to the continuation of three of the multiple solutions in the inviscid limit. In each of these neutral curves, the region within the loop is unstable and the region outside the loop is stable. For a given neutral curve, and for fixed Σ, there is a first transition from stable to unstable modes as Re is increased (when the 'lower branch' of the neutral curve is crossed), and there is a second transition from unstable to stable modes for a further increase in Re (when the 'upper branch' of the neutral curve is crossed). The lower branch of the neutral curves is obtained as a continuation from the results of the inviscid analysis of § 3.2, and the Reynolds number was decreased in the numerical continuation scheme. It is seen that the neutral curves do not extend to arbitrarily low values of Σ, and the continuation of the inviscid instability exists only up to a certain Σ below which the flow is stable. Our computations indicate that the critical and wall layers are not well-separated along the upper branch of the neutral curve in the (Re, Σ)-plane and they merge at high Reynolds numbers along the upper branch. In the inviscid asymptotic analysis of § 3.2, it was assumed that the critical and wall layers are well separated, and hence, the solutions of the upper branch in the high Reynolds number limit are not accessible to the present inviscid analysis. The inviscid solutions of § 3.1 were used to obtain only the lower branch of the neutral curve where the critical and wall layers are well separated.

In figure 7 neutral curves for different values of k are plotted for the case of $H = 2, n = 1, \eta_r = 0$. In this figure, we have plotted only the most unstable of the multiple solutions for each k. The most unstable mode for a given k is defined here as the neutral curve with the lowest value of transition Re below which the flow is stable. Also, we have plotted the neutral curves only for three different k for the sake of clarity. In the region between the loops there exist unstable regions of other axial wavenumbers k which are not shown in this figure. The most important neutral curve which gives the lower bound for instability is the curve whose lower branch has the minimum Re for a given Σ. This is because, for any fixed Σ, the region below this curve is stable to disturbances of all wavelengths and the region above the curve is

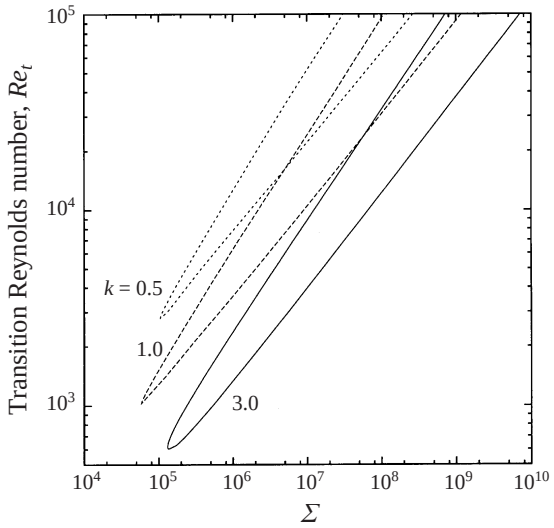

FIGURE 7. The neutral stability loops for different values of k: $H = 2, n = 1, \eta_r = 0$.

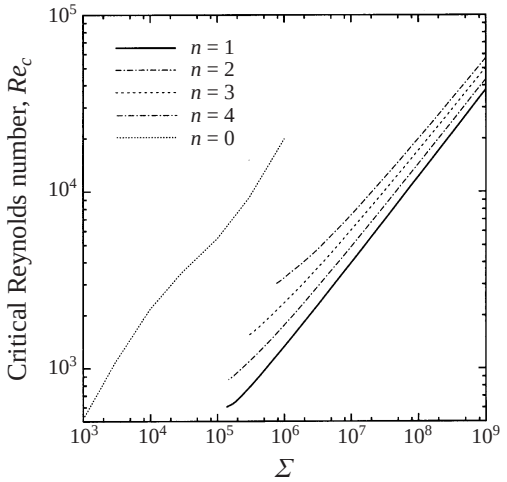

FIGURE 8. Comparison of present results for non-axisymmetric modes with the results from the axisymmetric ($n = 0$) viscous instability of Kumaran (1998*a*): critical Reynolds number vs. Σ for $H = 2$, $\eta_r = 0$. Only the lower branch of the neutral curves is plotted here.

unstable either due to this particular k, or due to instability to modes with other values of k. Consequently, for a given Σ, the lower branch with the smallest Re_t gives the critical Reynolds number above which the flow is unstable and below which the flow is linearly stable.

The critical Reynolds number curves (as defined above) for the continuation of non-axisymmetric inviscid modes are plotted in figure 8 for $H = 2$ and different values of n. It should be mentioned here that only the lower branch of these neutral curves is shown in this figure, since this information is sufficient to determine the critical Reynolds number below which the flow is completely stable. It should also be noted that in these curves, the continuation of the non-axisymmetric inviscid modes does not extend below $\Sigma \sim 10^5$ for $H = 2$. The critical Re curve obtained for the axisymmetric

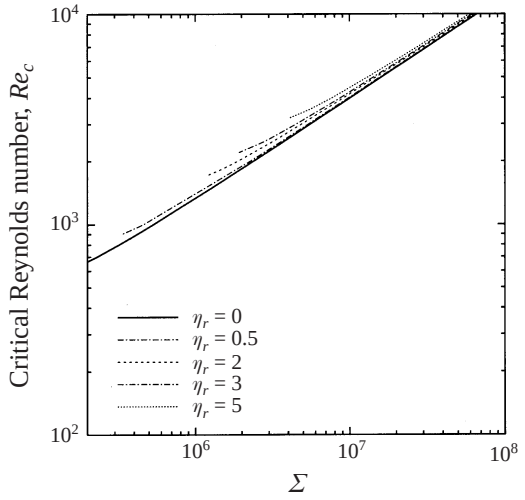

FIGURE 9. Effect of viscosity of the wall medium (η_r) on the neutral stability curves for azimuthal wavenumber $n = 1$. Only the lower branch of the neutral curves is plotted here.

viscous instability of the Hagen–Poiseuille velocity profile (Kumaran 1998*a*) is also plotted in the same figure for comparison. The critical *Re* curve for the viscous axisymmetric instability was obtained (Kumaran 1998*a*) as a numerical continuation of the viscous instability of Kumaran (1995*a*). This figure shows that the critical *Re* obtained for the continuation of the inviscid instability to non-axisymmetric modes is much lower than the critical *Re* of the viscous instability to axisymmetric modes for $\Sigma > 10^5$. Thus, this instability can be effective in the limit of moderate to high Σ. The inviscid instability does not exist for $\Sigma < 10^5$ for $H = 2$, and consequently for lower values of Σ, the viscous instability will be the important destabilizing mechanism. This plot also shows that the non-axisymmetric disturbance with azimuthal wavenumber $n = 1$ gives rise to the lowest critical *Re* for a given Σ. Thus, the continuation of the non-axisymmetric inviscid unstable mode with $n = 1$ is the most unstable mode for Hagen–Poiseuille flow in a flexible tube with $H = 2$. In figure 9, the effect of viscosity of the wall medium on the lower branch of the neutral curve is examined. This plot of critical Reynolds number vs. Σ shows that the critical Reynolds number increases as η_r is increased indicating that the viscosity of the wall medium has a stabilizing effect on this instability.

The numerical results obtained for a wall thickness of $H = 5$ are discussed next. The neutral curves for $H = 5$ show rather complex behaviour and it is first useful to mention the types of modes that are possible for non-axisymmetric disturbances. The main focus of this paper is on the continuation of the singular inviscid non-axisymmetric modes to moderate *Re*. However, at moderate *Re*, a continuation of the viscous non-axisymmetric mode could also exist. The viscous non-axisymmetric mode ($n \neq 0$) is qualitatively similar to the viscous axisymmetric modes ($n = 0$) analysed in Kumaran (1995*a*, 1998*a*), and these modes are obtained as a continuation from the $Re \to 0$ limit to moderate *Re*. Figure 10(*a*) shows two neutral curves in the (Re, Σ)-plane for $H = 5, n = 1, k = 3, \eta_r = 0$. In this figure, the neutral stability loop is the continuation of singular inviscid modes, and it has the same qualitative features as discussed above for the $H = 2$ case. The other curve which extends from $Re \to 0$ to $Re \sim 10^4$ is the continuation of the viscous mode for $n = 1, k = 3$.

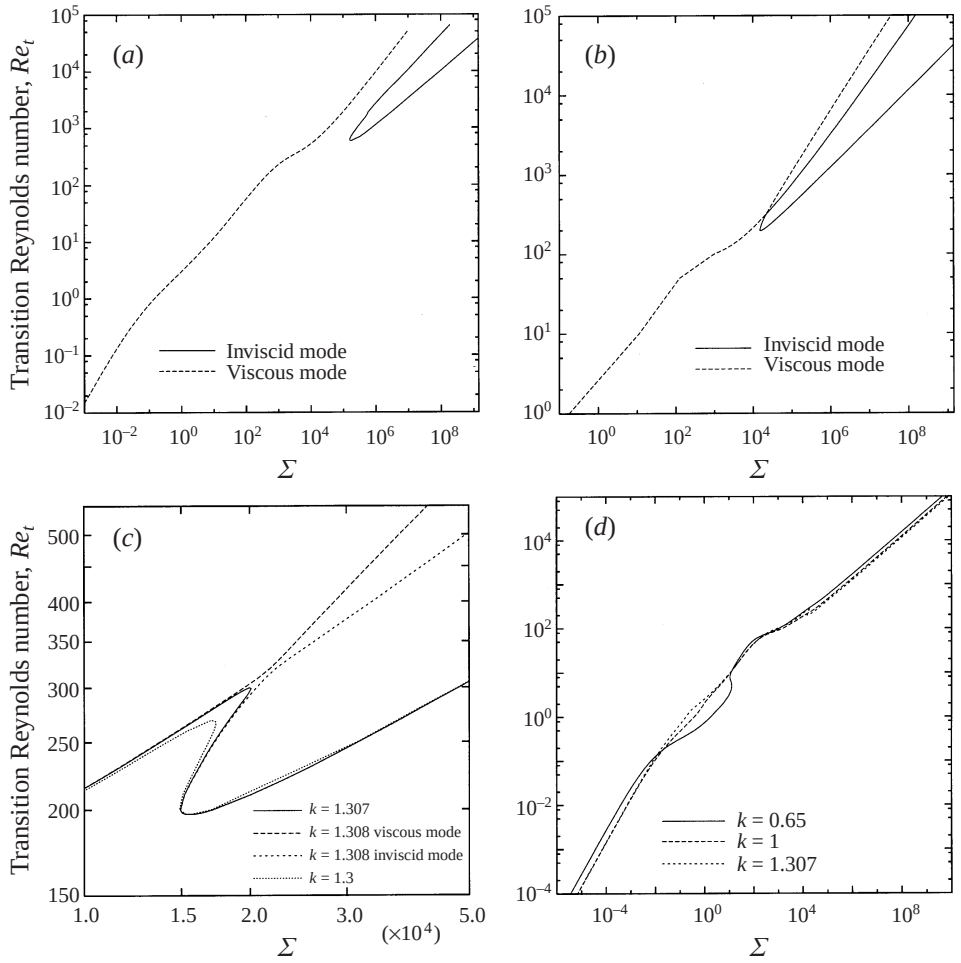

FIGURE 10. The neutral stability curves illustrating continuations of non-axisymmetric inviscid and non-axisymmetric viscous instabilities as k is varied for $H = 5, n = 1, \eta_r = 0$. (*a*) $k = 3$, viscous and inviscid modes are widely separated; (*b*) $k = 1.308$, the curves approach each other; (*c*) $k = 1.307, 1.308, 1.3$, the curves merge; (*d*) $k = 0.65, 1.0, 1.307$, for $10^5 < \Sigma < 10^{10}$, $Re \sim \Sigma^{1/2}$, while for $10^{-6} < \Sigma < 10^{-1}$, $Re \sim \Sigma$.

This figure illustrates that the neutral curve associated with the continuation of the inviscid mode appears at a much lower Re than the viscous neutral curve, and the continuation of the inviscid instability exists only for $\Sigma > 10^5$. This figure also shows that the non-axisymmetric viscous and inviscid modes are widely separated for $k = 3$. As k is decreased, however, the two modes intersect each other and merge together and give rise to a single neutral curve as illustrated in figures 10(*c*) and 10(*d*). Figure 10(*b*) shows the continuations of the singular inviscid mode and the viscous mode approaching each other for $k = 1.308$. In figure 10(*c*), the neutral curves for the viscous and inviscid instability for $k = 1.308$ are plotted along with the neutral curve obtained for $k = 1.307$ and $k = 1.3$. Only a part of the Re, Σ region is shown here for clarity. In this figure, for $k = 1.308$, there are two separate neutral curves corresponding to the continuations of singular inviscid and viscous modes. However, for $k = 1.307$ and $k = 1.3$, the neutral curve corresponding to the inviscid instability

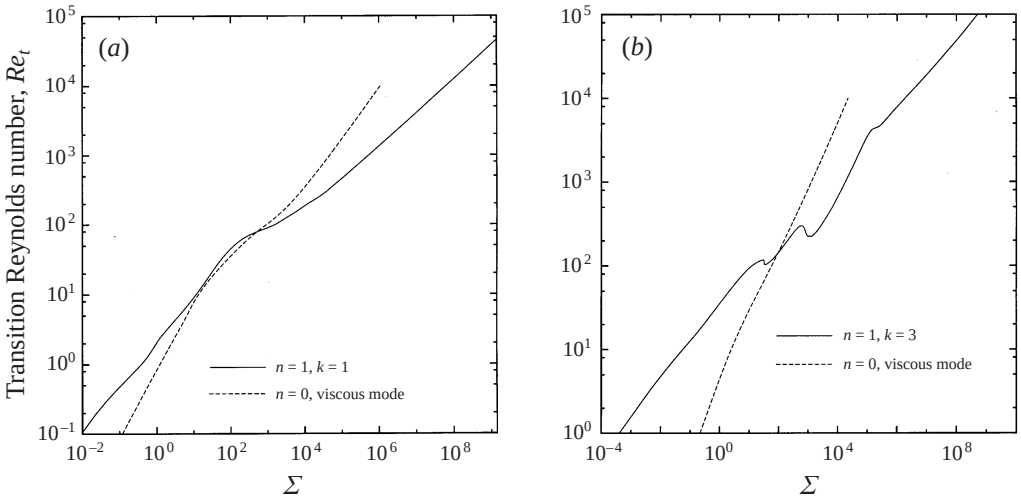

FIGURE 11. Comparison of neutral stability curves for the continuation of the non-axisymmetric inviscid instability ($n = 1, \eta_r = 0$) with the continuation of the axisymmetric viscous instability of Kumaran (1998*a*): (*a*) $H = 5, k = 1$; (*b*) $H = 1.2, k = 3$.

has merged with the neutral curve corresponding to the non-axisymmetric viscous instability, thus giving rise to a single neutral curve.

Further decrease in k yields a single neutral curve which extends over a wide range of Reynolds number as shown in figure 10(*d*). This figure shows neutral curves for three values of k, and for all the cases the neutral curves were continued from $Re = 10^5$ using the inviscid asymptotic results as starting guesses. It can be seen that neutral modes continue from $Re \sim 10^5$ to $Re \sim 10^{-4}$. When $10^5 < \Sigma < 10^{10}$, the scaling relation along the neutral curve is $Re \sim \Sigma^{1/2}$ characteristic of the inviscid modes, and when $10^{-6} < \Sigma < 10^{-1}$, $Re \sim \Sigma$ which is characteristic of the viscous modes. In figure 11(*a*), the neutral curve obtained for $n = 1, k = 1, H = 5$ obtained in this paper is plotted along with the neutral curve of the most unstable mode obtained as a continuation of the viscous axisymmetric neutral curve of Kumaran (1998*a*) for $H = 5$. This figure shows that for $\Sigma > 10^3$, the neutral curve obtained in this paper has much lower critical Reynolds number, while for $\Sigma < 10^3$ the neutral curve obtained in Kumaran (1998*a*) has a lower critical Reynolds number. Thus, for $H = 5$, the instability analysed in this paper will be important for $\Sigma > 10^3$, while the axisymmetric viscous instability of Kumaran (1998*a*) will be important for $\Sigma < 10^3$. In figure 11(*b*), the neutral curve obtained in this paper is compared with that of Kumaran (1998*a*) for $H = 1.2$. The neutral curve corresponding to $n = 1$ was obtained as a continuation of the inviscid results of § 3.1, while the neutral curve for $n = 0$ was obtained as a continuation (Kumaran 1998*a*) of the viscous modes to the intermediate-Re regime. This figure again demonstrates that for high values of Σ ($\Sigma > 10^2$ in this case) the continuation non-axisymmetric inviscid instability has much lower critical Reynolds number than the axisymmetric viscous mode. For $\Sigma < 10^2$, however, the continuation of the axisymmetric viscous mode has a lower critical Re, and this would be the important destabilizing mechanism for such cases.

From the numerical results presented above, the following general picture emerges for the linear stability of parabolic flow in a flexible tube. The Hagen–Poiseuille flow in a flexible tube will become unstable to inviscid non-axisymmetric modes for tubes with large values of Σ. For smaller values of Σ, the continuation of the axisymmetric

viscous modes is the most unstable. The value of Σ at which this cross-over from inviscid instability mechanism to viscous instability mechanism occurs depends on H. For $H = 2$, the inviscid non-axisymmetric modes do not extend below a certain value of $\Sigma \sim 10^4$, and the axisymmetric viscous modes will destabilize the flow for small Σ. Even if the inviscid modes continue to very low values of Σ (as for $H = 5$ and $H = 1.2$), the critical Reynolds number of viscous axisymmetric modes is much lower than the inviscid modes for low values of Σ. Consequently, the inviscid non-axisymmetric modes analysed in this paper will be powerful in destabilizing the Hagen–Poiseuille flow in flexible tubes in situations where the dimensionless parameter Σ is large.

We now provide a brief comparison of the present work with some representative previous theoretical studies. In the limit $Re \gg 1$ and $\rho V^2/G \sim O(1)$, two classes of modes are possible in flow past flexible surfaces which are absent in the flow past rigid surfaces. The first class of modes is called the 'regular inviscid modes'. For these modes, there is a balance between the inertial forces in the fluid and elastic forces in the wall. In the limit of high Re, the flow is inviscid in the core of the tube, and there is a wall layer of thickness $O(Re^{-1/2})$ smaller than the tube radius where the viscous stresses are important. The destabilizing mechanism in this case is the work done by the pressure forces on the wall material. This type of instability has been observed in flows past walls made of spring-backed plates. Carpenter & Garrad (1985) studied the effect of wall compliance on the Tollmien–Schlichting instability that already exists in flow past rigid surfaces. The instability analysed in Carpenter & Garrad (1986) is a Kelvin–Helmholtz-type instability where the discontinuity of the mean velocity profile at the interface is the primary driving force. Asymptotic and numerical studies of regular inviscid modes have also been carried out by Carpenter & Gajjar (1990) for the case of a Blasius boundary layer past a compliant wall and Davies & Carpenter (1997) for the case of fully developed flow in a two-dimensional channel with compliant walls.

The unstable modes analysed in this paper are classified under 'singular inviscid modes'. For parabolic flow in a flexible tube subjected to non-axisymmetric disturbances, the leading-order inviscid stability equation contains a singularity when $Re \gg 1$, where the wave speed of the disturbances equals the local fluid velocity. Viscous effects become important in the critical layer of thickness $O(Re^{-1/3})$ and in the wall layer of thickness $O(Re^{-1/2})$. The physical mechanism driving the instability is the convective transport of energy from mean flow to fluctuations due to the Reynolds stresses in the critical layer. Critical layers are absent in the stability of Hagen–Poiseuille flow to axisymmetric disturbances (regular inviscid modes), and the flow is stable in the limit of high Re (Kumaran 1995*b*).

4. Conclusion

The stability of fluid flow in a flexible tube to non-axisymmetric disturbances was analysed using asymptotic and numerical methods. In § 2, the classical theorems of hydrodynamic stability concerning the temporal instability of inviscid flows over rigid walls were modified and extended to the case of inviscid flow through flexible tubes. The important results were stated in Propositions 1 to 6 in § 2. The only assumption made in deriving these theorems is that the laminar velocity profile is axisymmetric, and reduces to zero at the wall of the tube. Since a Squire-like theorem cannot be derived for axisymmetric geometries, it is necessary to consider non-axisymmetric disturbances when analysing the stability in such geometries. For the practically

important case of Hagen–Poiseuille flow, the general results predict that the flow is always stable to axisymmetric disturbances, but could be unstable in the inviscid limit to non-axisymmetric disturbances with any non-zero azimuthal wavenumber. An important result on the bounds of the real part of the wave speed c_r for unstable modes is that $U_L < c_r < U_U$; here U_L is the smaller of the minimum of the base flow velocity and zero, and U_U is the larger of the maximum of the base flow velocity and zero. For mean flows which satisfy the no-slip condition at the wall and vary monotonically towards the centre of the tube, the bounds on c_r reduce to $0 < c_r < U_{\max}$. When $0 < c_r < U_{\max}$, the point at which $c_r = U$ is a regular singular point, and there is an associated critical layer where viscous effects are important (Drazin & Reid 1981). The bound on c_r obtained in the present work indicates that the unstable modes in the inviscid limit are the singular modes for velocity profiles that vary monotonically from the wall to the centre. These general results can be used in identifying potentially unstable velocity profiles, and the bounds on the wave speed can be used as a guide in the numerical search for unstable modes at high Reynolds number.

The stability of the Hagen–Poiseuille flow in a flexible tube to non-axisymmetric disturbances was analysed in the limit of high *Re* using an asymptotic analysis. This analysis showed that the flow is unstable in the inviscid limit, and this is in agreement with the prediction of Propositions 1 and 2 derived in this paper. A numerical procedure was used to continue these inviscid modes to lower *Re* by solving the complete governing equations. Results from this numerical solution show that the continuation of the inviscid instability can persist even at very moderate *Re*. Comparison with the results of Kumaran (1998*a*) shows that the critical *Re* for the continuation of the non-axisymmetric inviscid instability could be far lower than the critical *Re* of the axisymmetric viscous instability when the dimensionless parameter characterizing the flexible tube, $\Sigma \equiv \rho G R^2/\eta^2$, is large. The viscosity of the wall medium is found to have a stabilizing influence on this instability. In conclusion, the present study shows that the instability of the fluid flow to non-axisymmetric disturbances could be practically important in initiating the transition in flexible tubes when the dimensionless parameter Σ is large. It is useful to estimate the value of Σ in a typical application, in order to determine the applicability of the regime $\Sigma \gg 1$. The shear modulus G varies in the range 10^2–$10^3\ \mathrm{N\,m^{-2}}$, the lower value being typically encountered in soft biological tissues while the upper limit is applicable to dense polymer gels. The viscosity of fluids and biological suspensions is typically in the range 10^{-2}–$10^{-3}\ \mathrm{N\,s\,m^{-2}}$, while the density of most liquids is about $10^3\ \mathrm{kg\,m^{-3}}$. Using the above values, Σ can be estimated as $\Sigma \sim 10^{11} R^2$. Even when $R \sim 10^{-3}$ m, $\Sigma \sim 10^5$. Thus, the present instability is expected to be encountered in flexible tubes with radii of $O(1\,\mathrm{mm})$ and higher.

REFERENCES

Batchelor, G. K. & Gill, A. 1962 Analysis of the stability of axisymmetric jets. *J. Fluid Mech.* **14**, 529–551.

Carpenter, P. W. & Gajjar, J. S. B. 1990 A general theory for two and three dimensional wall-mode instabilities in boundary layers over isotropic and anisotropic compliant walls. *Theor. Comput. Fluid Dyn.* **1**, 349–378.

Carpenter, P. W. & Garrad, A. D. 1985 The hydrodynamic stability of flows over Kramer-type compliant surfaces. Part 1. Tollmien-Schlichting instabilities. *J. Fluid Mech.* **155**, 465–510.

Carpenter, P. W. & Garrad, A. D. 1986 The hydrodynamic stability of flows over Kramer-type compliant surfaces. Part 2. flow induced surface instabilities. *J. Fluid Mech.* **170**, 199–232.

Davies, C. & Carpenter, P. W. 1997 Instabilities in a plane channel flow between compliant walls. *J. Fluid Mech.* **352**, 205–243.

Drazin, P. & Reid, W. 1981 *Hydrodynamic Stability*. Cambridge University Press.

Garg, V. K. & Rouleau, W. 1972 Linear spatial stability of pipe Poiseuille flow. *J. Fluid Mech.* **54**, 113–127.

Harden, J., Pleiner, H. & Pincus, P. 1991 Hydrodynamic surface modes on concentrated polymer solutions and gels. *J. Chem. Phys.* **94**, 5208–5221.

Howard, L. N. & Gupta, A. S. 1962 On the hydrodynamic and hydromagnetic stability of swirling flows. *J. Fluid Mech.* **14**, 463–476.

Kumaran, V. 1995*a* Stability of the viscous flow of a fluid through a flexible tube. *J. Fluid Mech.* **294**, 259–281.

Kumaran, V. 1995*b* Stability of the flow of a fluid through a flexible tube at high Reynolds number. *J. Fluid Mech.* **302**, 117–139.

Kumaran, V. 1996 Stability of an inviscid flow through a flexible tube. *J. Fluid Mech.* **320**, 1–17.

Kumaran, V. 1998*a* Stability of fluid flow through a flexible tube at intermediate Reynolds number. *J. Fluid Mech.* **357**, 123–140.

Kumaran, V. 1998*b* Stability of wall modes in a flexible tube. *J. Fluid Mech.* **362**, 1–15.

Landau, L. & Lifshitz, E. 1989 *Theory of Elasticity*. Pergamon.

Lin, C. C. 1945 On the stability of two-dimensional parallel flows. *Q. Appl. Maths* **3**, 117–142, 218–234, 277–301.

Maslowe, S. 1974 Instability of rigidly rotating flows to non-axisymmetric disturbances. *J. Fluid Mech.* **64**, 307–317.

Salwen, H. & Grosch, C. 1972 The stability of Poiseuille flow in a pipe of circular cross-section. *J. Fluid Mech.* **54**, 93–112.

Shankar, V. 1999 Linear and nonlinear stability of fluid flow in a flexible tube. PhD Thesis, Indian Institute of Science, Bangalore, India.

Shankar, V. & Kumaran, V. 1999 Stability of non-parabolic flow in a flexible tube. *J. Fluid Mech.* **395**, 211–236.

Tong, Z. & Liu, X. 1993 Dynamic mechanical behaviour of polyelectrolyte gels with sulfonic acid groups. *Macromolecules* **26**, 4964–4966.

Yeo, K. 1994 Note on the inviscid stability of flow over a compliant wall. *J. Fluid Mech.* **279**, 165–168.

Yeo, K. & Dowling, A. 1987 The stability of inviscid flows over passive compliant walls. *J. Fluid Mech.* **183**, 265–292.